Available online at www.sciencedirect.com
ScienceDirect
Trans. Nonferrous Met. Soc. China 28(2018) 1763−1773
Transactions of Nonferrous Metals Society of China
www.tnmsc.cn

Osteogenic composite nanocoating based on nanohydroxyapatite, strontium ranelate and polycaprolactone for titanium implants

Murat Taner VURAT[1,2], Ayşe Eser ELÇIN[1], Yaşar Murat ELÇIN[1,2]

1. Tissue Engineering, Biomaterials and Nanobiotechnology Laboratory, Faculty of Science and Stem Cell Institute, Ankara University, Ankara 06100, Turkey;
2. Biovalda Health Technologies, Inc., Ankara 06830, Turkey

Received 16 October 2017; accepted 3 April 2018

Abstract: Titanium and its alloys are commonly used as dental and bone implant materials. Biomimetic coating of titanium surfaces could improve their osteoinductive properties. In this work, we have developed a novel osteogenic composite nanocoating for titanium surfaces, which provides a natural environment for facilitating adhesion, proliferation, and osteogenic differentiation of bone marrow mesenchymal stem cells (MSCs). Electrospinning was used to produce composite nanofiber coatings based on polycaprolactone (PCL), nano-hydroxyapatite (nHAp) and strontium ranelate (SrRan). Thus, four types of coatings, i.e., PCL, PCL/nHAp, PCL/SrRan, and PCL/nHAp/SrRan, were applied on titanium surfaces. To assess chemical, morphological and biological properties of the developed coatings, EDS, FTIR, XRD, XRF, SEM, AFM, in-vitro cytotoxicity and in-vitro hemocompatibility analyses were performed. Our findings have revealed that the composite nanocoatings were both cytocompatible and hemocompatible; thus PCL/HAp/SrRan composite nanofiber coating led to the highest cell viability. Osteogenic culture of MSCs on the nanocoatings led to the osteogenic differentiation of stem cells, confirmed by alkaline phosphatase activity and mineralization measurements. The findings support the notion that the proposed composite nanocoatings have the potential to promote new bone formation and enhance bone-implant integration.

Key words: osteogenic nanocoating; composite nanofiber; titanium implant; nanohydroxyapatite; strontium ranelate; polycaprolactone; electrospinning; mesenchymal stem cells

1 Introduction

Bone is a highly vascularized and dynamic organ that has a number of functions such as protection, mineral storage and source of hematopoietic and mesenchymal stem cells (MSCs). Chemically, bone tissue consists of 1% sodium chloride, 1%−2% magnesium phosphate, 1%−2% calcium fluoride, 7% calcium carbonate and 58% calcium phosphate. Bone tissue, known as osseous, is made of cancellous and cortical bone. Living bone is mainly composed of collagen (70%), bone mineral and water. In addition, organic materials such as polysaccharides, proteins and lipids are present in less amounts [1,2]. Bone healing is a complex process with three distinct overlapping steps: early inflammatory stage, repair stage and the late remodeling stage [3,4]. Initially, within few days a local hematoma develops at the fracture site. Cellular inflammatory elements such as lymphocytes, monocytes, macrophages, and polymorphonuclear cells infiltrate the hematoma to secrete cytokines and growth factors. In the repair stage, fibroblasts facilitate vascular ingrowth and there is high osteoblast activity. At this stage, the newly formed bone needs to be remodeled. The last stage of bone tissue healing is the remodeling stage where bone is restored to its healthy condition [5,6].

The coating of orthopaedic implants or bone fixator surfaces aims to improve the implant-bone integration, restore tissue functions and accelerate bone healing. An ideal implant surface coating should mimic the bone tissue by being biocompatible, osteoinductive, and mechanically stable [6].

Due to their high corrosion resistance, unique mechanical properties, osseointegration capacity and high biocompatibility with the tissue, titanium and its alloys are widely preferred in the dental and orthopaedic implant applications [7,8]. Owing to their lack of direct

Corresponding author: Yaşar Murat ELÇIN; E-mail: elcinmurat@gmail.com; elcin@ankara.edu.tr
DOI: 10.1016/S1003-6326(18)64820-4

chemical bonding capacity with the tissue, titanium alloys are bioinert materials. Some surface modifications are applied to titanium alloys for providing better implant integration. Metals and their alloys are coated with various biocompatible materials for biomedical applications. Some coating techniques, such as sol−gel, thermal spraying, sputtering, dipping and immersion coating, and electrophoretic deposition, were used in previous works [9]. Besides, the electrospininng process is used in many biomedical applications. Electrospinning is useful for manufacturing non-woven polymer fibers with diameters in the range of submicrometers to nanometers [10−12].

Polycaprolactone (PCL) is a prominent polymer which has been widely used in biomedical applications, due to its non-toxicity, good mechanical properties, slow degradation rate, low-cost and high biocompatibility. PCL has high thermal stability with a melting temperature of 58−60 °C, and a glass transition temperature of −60 °C. Also, PCL has already been approved for use as a biomaterial for a number of applications by the FDA. In addition to these advantages, electrospun PCL nanofibers could mimic the extracellular matrix (ECM) of many tissues [13−17].

Chemical composition and physical structure of hydroxyapatite (HAp) are very similar to those of the natural bone, hence, HAp has been used in hard tissue engineering studies alone or as a biomaterial component [18−20]. Additionally, HAp has been used as a coating material for implant applications owing to its good biocompatibility, osteoconductivity and bioactivity [21,22]. HAp displays high binding capacity to bone and enhances bone tissue formation.

Strontium is an essential trace element with bioactive properties related to the skeletal metabolism. Recent in-vitro and in-vivo studies have reported the unique beneficial properties of strontium ions on bone healing [23−25]. Supporting this notion, recent work has shown that strontium induces MSC differentiation and pre-osteoblast proliferation, while also contributing to bone homeostasis by inhibiting osteoclast activity [26]. More previous researches elucidated the mechanism of strontium on the differentiation of osteoprogenitor cells into bone-forming osteoblasts through regulation of Wnt/β-catenin signalling pathway and expression of membrane-bound calcium sensing receptor (CaSR) [27,28]. Further evidence supports the role of strontium in bone anabolism, i.e., inducing the decrease in osteoclastogenesis, hence significantly lowering resorption activity of mature osteoclasts [29,30]. Also, chemical and physical structures of strontium are similar to those of calcium and about 98% of the total body strontium content is localized in the bone tissue [31].

Strontium ranelate (SrRan), a strontium chelating agent, is widely used for reducing bone fractures in high risk patients and for the treatment of osteoporosis, especially in postmenopausal women. In-vitro experiments have indicated a unique positive effect of SrRan on the bone tissue [32]. Also, SrRan can decrease osteoclast differentiation and promote osteoblast proliferation and activity. It also regulates osteoclast activity by editing the RANK, RANKL, OPG ratio and inhibits the secretion of TNF-α and IL-6 cytokines [33−35]. Despite, SrRan has not been proven to be effective in the treatment of rat femoral defects as a systemic treatment agent [36]; it has promising implications as a supporting component of tissue engineered implants. Titanium implant surfaces coated with SrRan-laden chitosan films have shown to promote osteoblast differentiation and proliferation in a dose-dependent fashion [37]. Similarly, mesoporous bioactive glass implants incorporated with strontium induce osteogenic activity and fracture repair through local release of Sr, which supports the incorporation of Sr in the composition of tissue engineered scaffolds for the treatment of bone defects [38,39].

Thus, the present study was designed to develop a composite osteogenic nanocoating for titanium surfaces, based on the electrospinning technique, and optimization of the polycaprolactone, hydroxyapatite, and strontium ranelate composition.

2 Experimental

2.1 Materials

Titanium foils (0.25 mm in thickness; ≥98%), were purchased from Goodfellow Corporation (Huntingdon, England). Polycaprolactone (M_w, 80000), hydroxyapatite nanopowder (<200 nm) and strontium ranelate (≥98%) were purchased from Sigma Aldrich (St. Louis, MO, USA). Dichloromethane was obtained from Merck (Darmstadt, Germany). Methanol was obtained from Sigma. In-vitro cytotoxicity and cell culture studies were performed using Dulbecco's modified Eagle's medium (DMEM; Lonza, Verviers, Belgium), supplemented with 10% fetal bovine serum (Lonza). Alizarin red dye was purchased from Sigma. All other reagents were used as cell culture grade from Sigma.

2.2 Preparation of titanium surfaces

Prior to the coating process, commercial titanium foils with 0.25 mm in thickness were cut into 10 mm × 10 mm pieces. Cleaning protocol was performed on the titanium surfaces. Titanium foils were initially washed with distilled water and then immersed in piranha solution (sulfuric acid/hydrogen peroxide, v/v; 70/30) in an ultrasonic bath for 15 min. Clean foils were ultra-sonicated in distilled water three times for 10 min.

Afterwards, the substrates were dried at room temperature. The cleaning performance of the protocol was evaluated via scanning electron microscopy (SEM) and atomic force microscopy (AFM) force−distance measurements.

2.3 Electrospinning

The polymer solution was prepared by dissolving PCL in DCM:MetOH (8:2, v/v) solvent mixture at a concentration of 10.0% (mass fraction). PCL was solubilized in this solvent mixture by the help of a vortex device. 5% nHAp and 2.5% SrRan were dispersed in PCL solution and sonicated at room temperature for 30 min. This procedure was also applied to other solutions. The studies were continued with four different experimental groups, as shown in Table 1.

Table 1 Contents of four types of nanofiber coatings on titanium substrates (Electrospinning conditions: voltage 20 kV; flow rate 0.2 mL/min; distance between tip and collecting plate 23 cm)

Type	*w*(PCL)/%	*w*(nHAp)/%	*w*(SrRan)/%
PCL	10.0	−	−
PCL/HAp	10.0	5.0	−
PCL/SrRan	10.0	−	2.5
PCL/HAp/SrRan	10.0	5.0	2.5

Electrospinning was performed using a lab-made device. The resulting composite solution was loaded into 5 mL plastic syringe attached to stainless-steel 21G needle. Briefly, the electrospinning process was carried out at an injection rate of 0.2 mL/min. Working distance between the fiber collector (titanium foil) and the needle was 23 cm, and a voltage of 20 kV was applied by using a high voltage power supply (Glassman PS/FC 60P02, High Bridge, NJ, USA) [40].

2.4 Characterization

A number of methods were utilized to characterize the properties of the titanium surfaces. SEM, AFM, energy-dispersive X-ray spectroscopy (EDS), X-ray diffraction spectroscopy (XRD), X-ray fluorescence spectroscopy (XRF), Fourier transform infrared spectroscopy (FTIR) were used to analyze the chemical and morphological properties. In-vitro cytotoxicity, in-vitro hemocompatibility, alkaline phosphatase activity and calcium assays were used to analyze the biological properties. Also, alizarin red staining was performed to determine the presence of calcific deposition.

2.4.1 SEM, EDS and AFM analyses

The morphological evaluation of nanofiber coatings and surface topography was performed by using a Quanta 400F model scanning electron microscope (FEI Instruments, Hillsboro, OR, USA). Gold coating of the samples was performed with an automatic sputter coater for 60 s. The average diameter of the electrospun nanofibers was determined by measuring the images of 30 fibers retrieved from three separate electrospinning experiments.

The general morphology and the structure of the nanofibers-coated titanium substrates were evaluated by nanomagnetic instruments AFM (Nanomagnetics Instruments, Ankara, Turkey).

2.4.2 FT-IR, XRD and XRF analyses

Chemical analysis was carried out by using a Spectrum 100 FT-IR spectrometer (Perkin Elmer, Waltham, MA, USA). Spectral findings were collected in the wavelength range of 4000−600 cm^{-1}, with a resolution of 16 cm^{-1} at 64 scans.

The crystalline structure of the coatings was analyzed by using a Rigaku D/Max 2200 model X-ray diffractometer (Tokyo, Japan), with Cu target and K_α radiation at a scanning rate of 4 min^{-1}, and 1540 Å K_α.

The elemental analyses of the nanocoatings were carried out with an ARL Perform'x model XRF spectrometer (Thermo Scientific, Waltham, MA, USA). Samples were prepared as disc-shaped, with 3 cm in diameter.

2.4.3 In-vitro cytotoxicity (ISO 10993-5)

Cytotoxicity testing was performed using the MTT (3-(4,5-dimethylthiazol-2-yl)-2,5-diphenyltetrazolium bromide) assay for quantification of the amount of viable cells. Extracts were prepared according to ISO 10993-5 using DMEM F−12 (Lonza, Basel, Switzerland) serum free medium. Surface area of each titanium specimen used in the extract experiment was 2.0 cm^2/mL. The negative control group consisted of DMEM F12 medium, while for positive control group we used 400 mmol/L phenol. Human fibroblast cells were incubated inside 24-well culture plates at a density of 5×10^4 cell/well. Cell culture was maintained at 37 °C and 5% CO_2 in humidified atmosphere. After incubation, medium was disposed and culture area was washed with PBS. We added serum free DMEM (270 μL) and MTT kit (30 μL) to each well and re-incubated for 4 h. Finally, we performed colorimetric measurements with formazan dye by using a SpectraMax M2 model multiplate reader (Molecular Devices, Sunnyvale, CA, USA).

2.4.4 In-vitro hemocompatibility (ISO 10993-4)

In-vitro hemocompatibility/hemolysis tests were performed on four samples according to the ISO 10993-4 standard. Samples were placed inside 15 mL tubes and 2 mL of diluted blood was added to each tube. The test was performed using fresh blood diluted with PBS as the negative control, and distilled water-diluted blood was used as positive control. Control groups and samples were incubated at 37 °C for 2 h. After the incubation

stage, blood samples were centrifuged at 1500 r/min for 10 min. The spectrophotometric measurement of the supernatants was performed at 545 nm.

2.4.5 Osteogenic cell culture

Rat bone marrow mesenchymal stem cells (BM-MSCs) were isolated from the femurs of adult Wistar rats ((275±25) g), and expanded as previously reported [41,42]. Cells at the 2nd passage were seeded on bare and nanofibers-coated titanium substrates at a density of 4×10^4 cell/cm^2 inside 12-well culture plates. Then, they were cultured in DMEM containing 10% FBS, 1% penicillin–streptomycin and 2 mmol/L *L*-glutamine (all from Sigma), at 37 °C with humidified 5% CO_2. When cells reached ~80% confluence (within 1−2 d), the medium was switched to the osteogenic medium (same medium containing 50 mg/mL ascorbic acid, 10 mmol/L Na-β-glycerophosphate, and 1×10^{-8} mol/L dexamethasone). Osteogenic BM-MSC cultures were maintained with fresh medium which was changed twice per week, for up to four weeks. Samples (collected media and cell cultures on titanium substrates) were retrieved at set time points for further analyses.

2.4.6 Alizarin red staining

Alizarin red staining was performed to determine the amount of calcific deposition of cells on nanofiber substrates. After 7, 14, 21 and 28 d of osteogenic culture, samples from each group were collected and washed three times in PBS and fixed with 2.5% glutaraldehyde. Fixed substrates were washed three times with distilled water and later stained with alizarin red S (Sigma) solution at pH 4.2. After staining, the samples were imaged and investigated macroscopically.

2.4.7 Alkaline phosphatase activity

Quantitative concentration of ALP can be used as an index for evaluating bone formation and bone diseases. The ALP activity was determined on medium samples collected during the osteogenic cell culture study, using the Quantichrom ALP Assay Kit (Bioassay Systems, Hayward, CA, USA). This assay is based on the fundamental principle of enzymatic conversion of *p*-nitrophenyl phosphate to *p*-nitrophenol and phosphate products. Absorbance of *p*-nitrophenol was measured by using a SpectraMax M2 model microplate reader (Molecular Devices) at a wavelength of 410 nm, and the enzyme activity was estimated from a *p*-nitrophenol standard curve.

2.4.8 Calcium assay

Calcium assay was performed by using the Quantichrom Calcium Assay Kit (DICA−500, Bioassay Systems) using collected media on the 14th and 28th days, according to the manufacturer's instructions. Phenolsulphonephthalein dye in the kit forms a blue colored complex with free calcium. Optical density was measured at a wavelength of 612 nm by using a Spectramax M5 model spectrophotometer (Molecular Devices). A standard curve was used to calculate calcium content.

2.5 Statistical analysis

For statistical analysis, all data are expressed as mean ± standard deviation. Unless stated otherwise, all experiments were repeated in triplicates. Statistical significance was defined as $p<0.05$. The results of the experiments were analyzed by using Student's *t*-test for calculating the degree of significance.

3 Results and discussion

3.1 Titanium surface characterization

Performance of the cleaning protocol was evaluated via SEM, AFM and AFM force−distance analysis before the electrospinning process. According to the obtained data, cleaning protocol was successful in terms of attaining surface homogeneity and removal of the inactive metal oxide layer. The SEM micrographs of titanium foil surfaces are shown in (Figs. 1(a_1)−(a_3)). As can be seen, untreated titanium surfaces are high in impurities and have an uncontrolled oxide layer. After the cleaning procedure, the entirety of the impurities and most of the oxide residues and elevations were removed successfully (Figs. 1(a_4)−(a_6).

Further analysis of surfaces indicated similar results with the SEM findings. AFM and AFM force−distance analyses support that the cleaned surfaces are generally homogeneous and free from impurities as shown in Figs. 1(b_3), (b_4) and 1(c_2), respectively. The roughness of the titanium surfaces (Figs. 1(b_1) and (b_2)) disappeared following the cleaning procedure, and showed a homogenous appearance as seen in Figs. 1(b_3) and (b_4). AFM force−distance analysis of the cleaned titanium surface is in line with the SEM and AFM findings. Approach and attract curves shown in Fig. 1(c_2) display proximity and significant similarities each other.

3.2 Electrospun nanofiber characterization

The morphological evaluation of the PCL, PCL/nHAp and PCL/nHAp/SrRan composite nanofiber coatings was performed with SEM and AFM. SEM micrographs revealed that titanium substrate had a highly porous surface, and after the coating process, the produced nanofibers were homogenous as shown in Fig. 2. Elemental composition of the coatings was analyzed by using EDS and XRF. In accordance with the obtained data, composite nanocoatings include titanium, calcium, phosphorus and strontium.

Figure 2 shows the SEM images of the PCL, PCL/nHAp and PCL/nHAp/SrRan composite nanofiber coatings at different magnifications. These surfaces

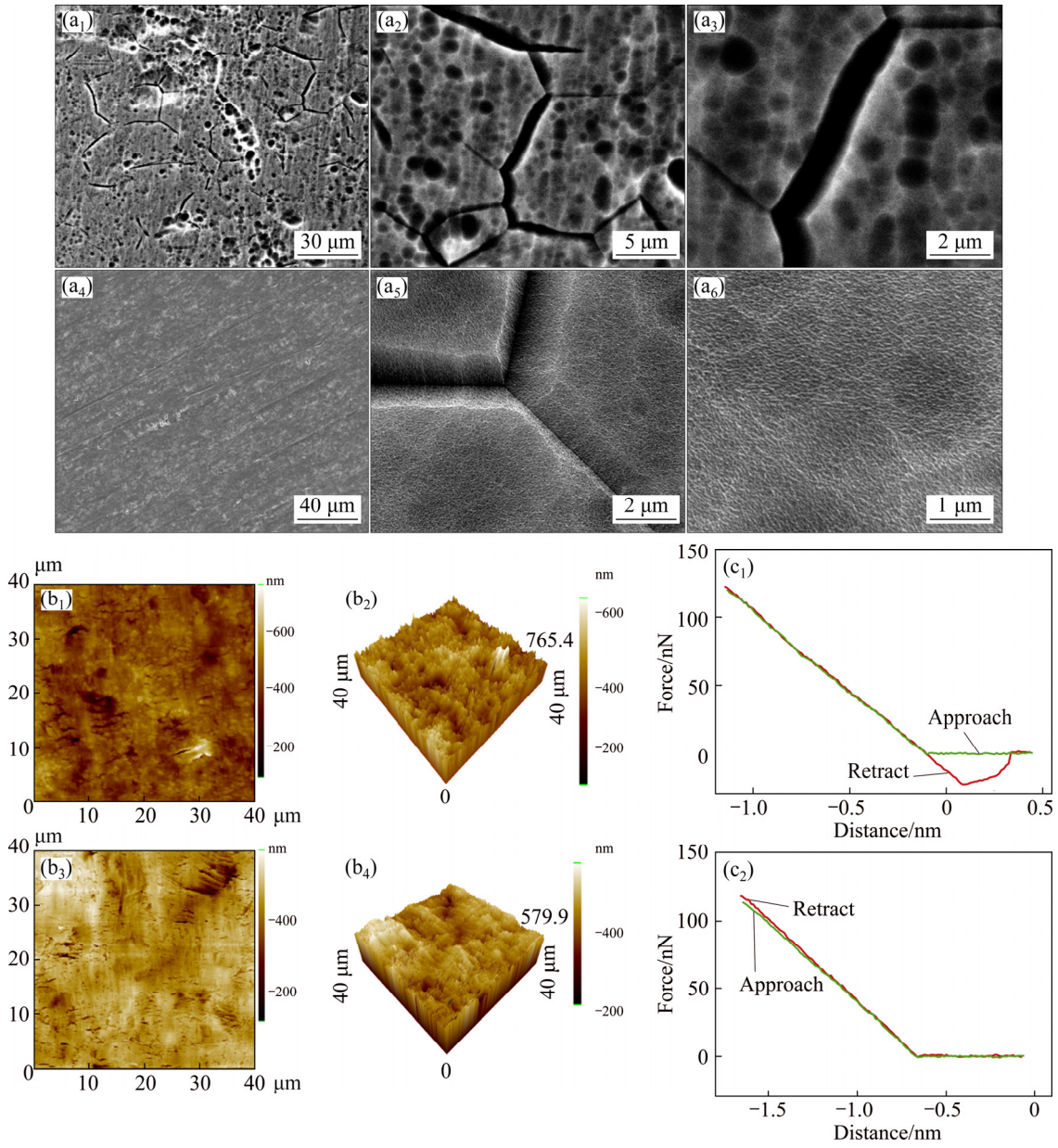

Fig. 1 SEM images of uncured titanium (a_1−a_3) and cleaned titanium (a_4−a_6) surfaces, 2D (b_1, b_3) and 3D (b_2, b_4) AFM micrographs of uncured titanium (b_1, b_2) and cleaned titanium (b_3, b_4) surfaces, and force−distance diagrams of uncured titanium (c_1) and cleaned titanium (c_2) samples

consist of homogeneous, bead free and morphologically similar nanofibers. As seen in Figs. 2(c)−(f), HAp nanoparticles were embedded within the PCL nanofibers. PCL/nHAp/SrRan nanofibers have an average diameter of (130±20) nm without any sign of bead formation. Homogeneous nanofibers were obtained and the particles were successfully embedded in the fiber structure in line with the previous study of VENUGOPAL et al [43].

The results of the SEM−EDS analysis showed that the calcium content was 24.62% and the phosphorus content was 13.75% (Fig. 3). Ca/P mass ratio of developed nanocoating was measured to be 1.79. The results of the qualitative SEM−EDS characterization experiments with PCL/nHAp/SrRan coated titanium substrates also ascertained the presence of titanium, calcium, phosphorus and strontium elements, as seen in Fig. 3.

We performed X-ray fluorescence spectrometer to obtain quantitative elemental chemical composition of the proposed nanocoating. The results of XRF analysis of the nanocoated titanium sample are presented in Table 2. As expected, titanium, calcium, phosphorous and strontium are the main components of the sample. Also, sodium, potassium, silicium, vanadium, chlorine, iron, barium, and nickel are present, along with impurities of titanium and HAp. According to XRF data, the

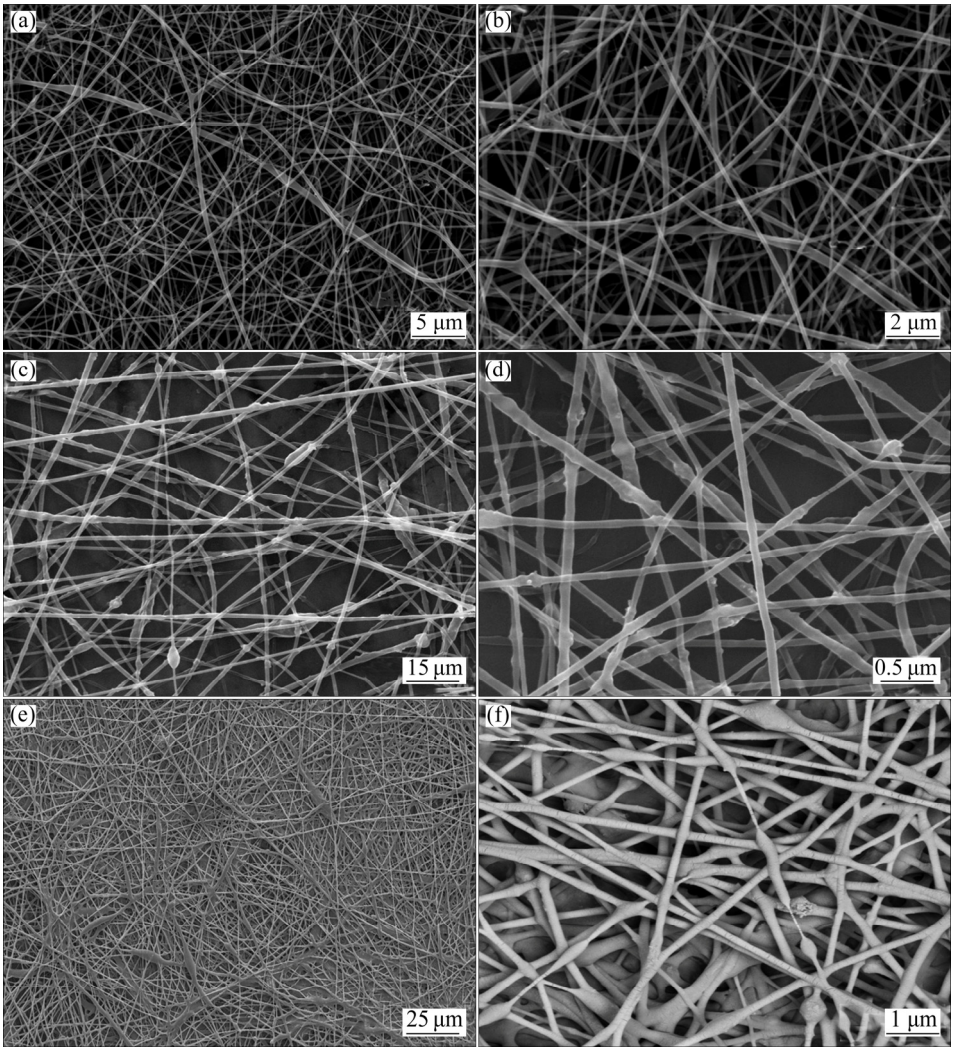

Fig. 2 SEM micrographs of 10% PCL (a, b), PCL/nHAp (c, d) and PCL/nHAp/SrRan (e, f) composite nanofiber coated titanium samples

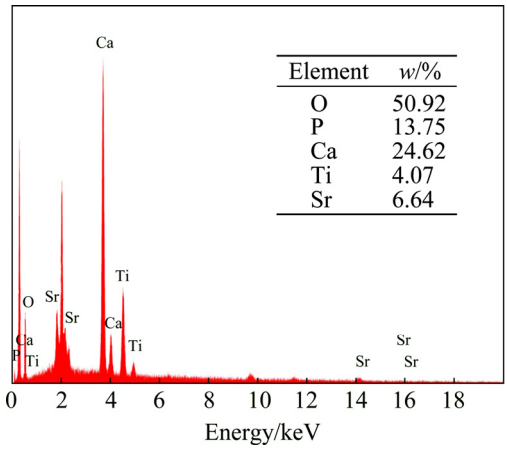

Fig. 3 EDS results of PCL/nHAp/SrRan composite nanofiber coated titanium samples

Ca/P mass ratio was 1.61. Ca/P mass ratio is in close agreement with the stoichiometric value for hydroxyapatite (1.67), also underlined by CAMARGO et al [44].

Table 2 Elemental compositions (XRF analysis) of PCL/HA/SrRan composite nanofibers

Element	Mass fraction/%
Titanium	52.45
Phosphorus	2.85
Calcium	4.6
Strontium	2.67
Sodium, potassium, silicium, Vanadium, chlorine, iron, barium, nickel	0.275

XRD patterns of the PCL, PCL/nHAp, PCL/SrRan and PCL/nHAp/SrRan nanofiber coatings are given in Fig. 4(a). XRD spectrum of PCL exhibited sharp diffraction peak at 2θ values of 21.4° and relatively low intensity peak at 23.6°. These angle values are characteristic peaks of the PCL [45,46]. On the other hand, XRD patterns of PCL/nHAp and PCL/nHAp/

SrRan composite nanofiber coatings indicated that hydroxyapatite was present in these samples shown by distinct characteristic HAp peaks appearing at 2θ values of 25.9°, 32°, 33°, 34° and 40°. In addition, there was no peak at 2θ of 39°, which is the carbonate-specific peak. This shows that the used nHAp did not contain carbonate impurities, which was an issue for other works in the related literature [47].

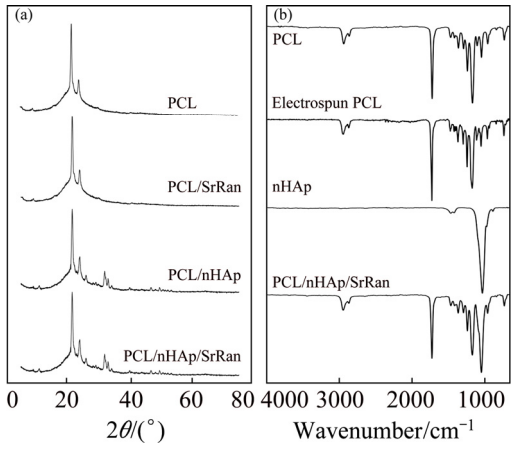

Fig. 4 XRD patterns of PCL, PCL/nHAp, PCL/SrRan and PCL/nHAp/SrRan nanofiber coated foils (a) and FT-IR spectra of PCL, electrospun PCL, nHAp and PCL/nHAp/SrRan nanofiber coated foils (b)

Functional groups associated with PCL and nHAp were investigated by FT-IR analysis. Figure 4(b) shows the FT-IR spectra of PCL, electrospun PCL, nHAp and PCL/nHAp/SrRan composite nanocoated titanium alloy. In the PCL and electrospun PCL spectra, we can identify the bands such as asymmetric —CH_2 stretching around 2965 cm^{-1}, symmetric —CH_2 stretching around 2870 cm^{-1}, carbonyl streching around 1730 cm^{-1}, asymmetric C—O—C stretching around 1250 cm^{-1} and symmetric C—O—C stretching around 1175 cm^{-1} [48,49]. Comparison of FT-IR spectra findings of electrospun PCL constructs and PCL in pellet form shows that there is no difference in the functional groups present after-electrospinning (Fig. 4(b)). These spectral findings show that the electrospinning process does not adversely affect the amount of functional groups present in the structure. PCL reveals the C—H peaks present at 1730 and 2850 cm^{-1} and C—O—C peaks at 1250 cm^{-1}. The phosphate groups in pure HAp showed characteristic FT-IR bands around 970, 1030 and 1090 cm^{-1} (Fig. 4(b)) [44].

3.3 In-vitro cytotoxicity and hemocompatibility

Phase contrast light micrographs of the four experimental groups and the two control groups for in-vitro cytotoxicity assay are given in Figs. 5(a)−(f). Upon MTT cell proliferation assay, cells produced formazan in dark blue. Quantitative MTT cell viability assay data showed that cell viability was about 85% in comparison to the control as given in Fig. 5(g). We accepted the cell viability as 100% in the negative control group, while the cell viability was almost 0 in the positive control group. The in-vitro cytotoxicity assay of the PCL/HAp/SrRan composite nanofiber coating and other experiment groups, i.e., titanium, PCL and PCL/nHAp showed that none of them was toxic to human dermal fibroblast cells, according to the ISO 10993-5 standard.

In addition to in-vitro cytotoxicity, the in-vitro hemocompatibility experiment was also performed on PCL, PCL/nHAp, PCL/SrRan and PCL/nHAp/SrRan-coated titanium substrates. The results of the hemolysis experiments are summarized in Table 3. Percent hemolysis value of the positive control group was ~98.9%; this value was 0.26% for the negative control. In the experimental groups, in-vitro hemolysis values were close to each other, showing that the nanocoatings on titanium substrates did not cause toxic effects to the fresh blood, and were basically hemocompatible.

3.4 Osteogenic culture study

Alizarin red staining of the coating membranes showed calcific deposition after 7, 14, 21 and 28 d of culture, as seen in Fig. 6. Between four experiment groups, Alizarin red-positive nodule amounts were different. According to the staining results, Alizarin red positive nodules in PCL/nHAp/SrRan group were high, but there was no obvious difference between days in the same experimental group as seen in Fig. 6. In a similar study performed by CHEN et al [50], cross-sections of PCL and HA/TCP-PCL scaffolds were stained with Alizarin red and HA/TCP-PCL was shown to contain higher amount of calcium after 7 d. However, there was no difference between groups on days 14 and 21. Our finding showed that PCL/nHAp/SrRan group contained higher calcium amount in comparison to other groups since PCL/nHAp/SrRan coating stimulated cell proliferation, leading to the increase in the mineralization of culture environment. This underlines the osteogenic role of SrRan in MSC behavior and its effect on the modification of the environment for calcium phosphate mineralization. In a similar study performed by QUERIDO and FARINA [51], Sr^{2+} was shown to promote an increase in the formation of mineralized nodules in osteoblast cell cultures.

3.5 Alkaline phosphatase and calcium findings

ALP activity values of rat mesenchymal stem cells cultured on the nanocoatings are given in Fig. 7(a). ALP activity decreased in all experimental groups from day 14 to day 28. The increased bone-specific ALP activity

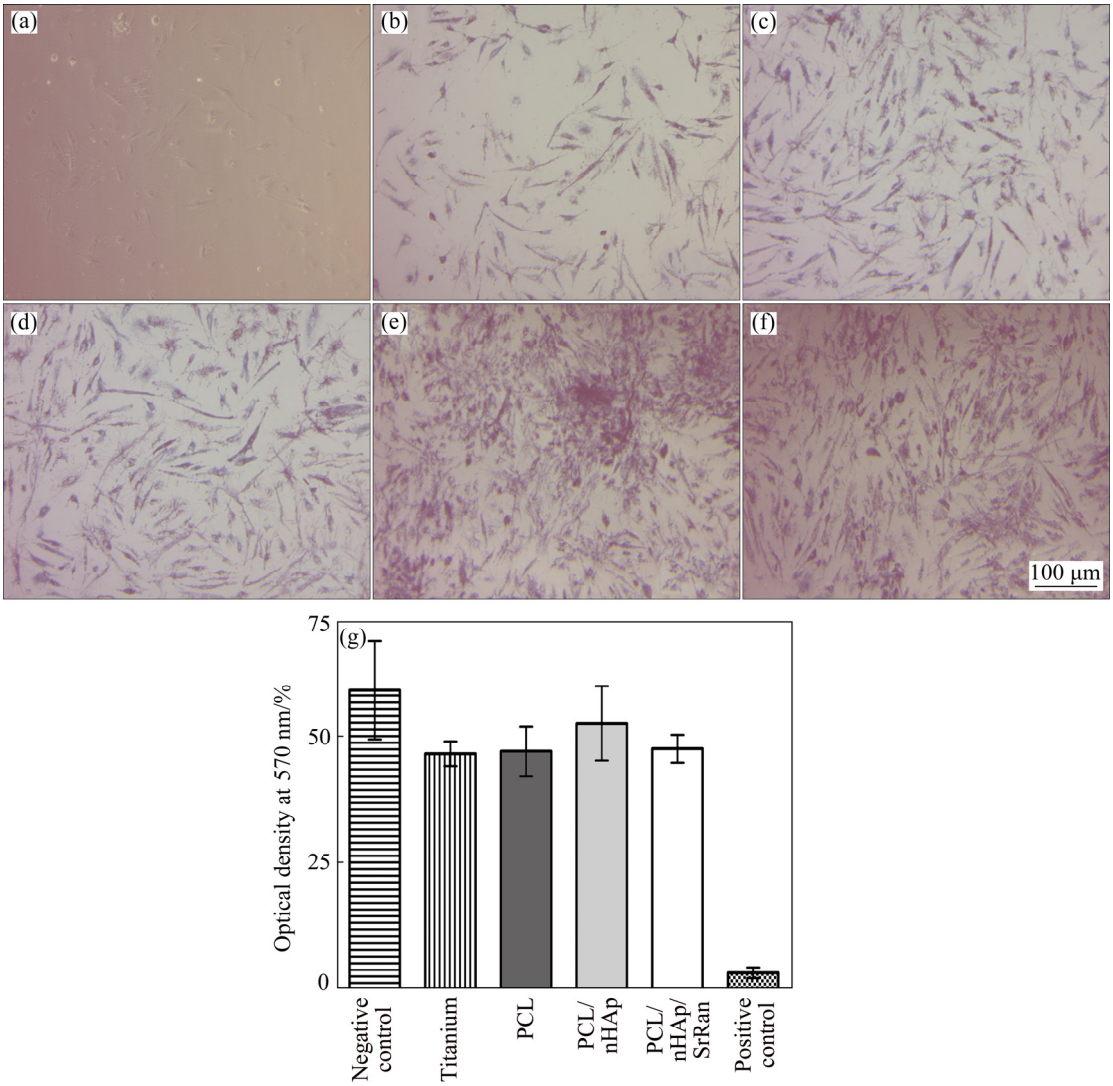

Fig. 5 Phase contrast micrographs (a−f) and MTT test results (g) of 4 experimental and 2 control groups for in-vitro cytotoxicity assay: (a) Positive control; (b) Bare titanium foil; (c) 10% PCL-coated titanium foil; (d) PCL/nHAp coated titanium foil; (e) PCL/nHAp/SrRan coated titanium foil; (f) Negative control; (g) MTT test results

Table 3 Hemolysis values of fresh blood interacted with samples

Group	Hemolysis/%
Positive control	98.9±0.2
Negative control	0.26±0.001
Titanium foil	0.29±0.001
PCL	0.39±0.001
PCL/HAp	0.38±0.002
PCL/SrRan	0.34±0.001
PCL/HAp/SrRan	0.29±0.001

in human serum is an indicator of known diseases such as hyperparathyroidism, osteosarcoma, osteoporosis and skeletal metastases [52]. As ALP assay is based on the detection of ALP activity released from the disrupted cells, the measured decrease in the growth medium

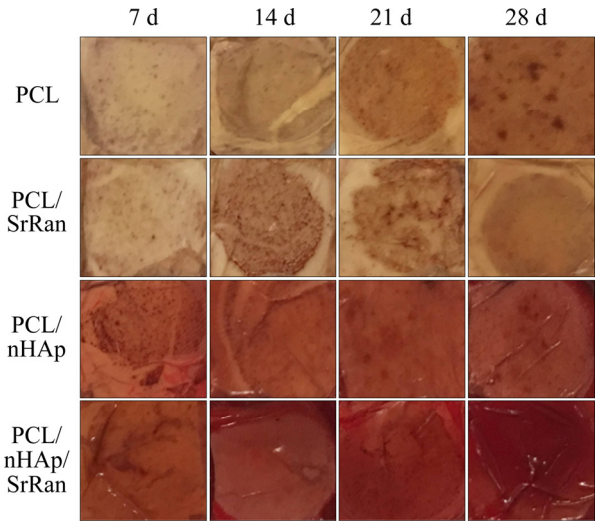

Fig. 6 Alizarin red stained osteogenic BM-MSC cultures on nanocoated titanium substrates retrieved at 7, 14, 21 and 28 d

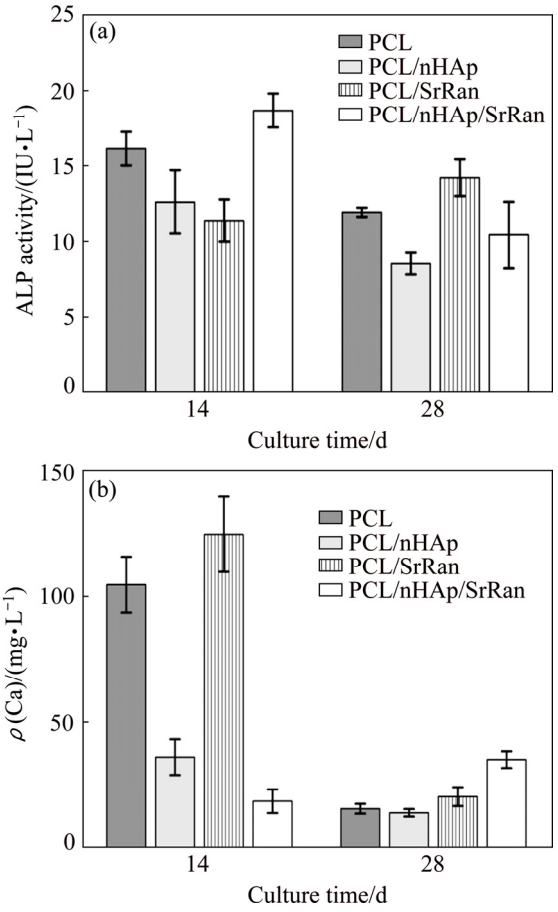

Fig. 7 Results of ALP activity assay after osteogenic culture of rMSCs (a) and time course experimental results to determine calcium content of osteogenic BM-MSC cultures (b)

indicates a decrease in the levels of cell loss through the duration of the study.

According to the calcium assay findings (Fig. 7(b)), similar to ALP results, medium calcium content of PCL, PCL/nHAp and PCL/SrRan groups decreased from day 14 to day 28. Only for PCL/nHAp/SrRan, calcium content showed a minor increase on day 28. This could be attributed to the higher rate of release of nHAp particles during the first 14 d of culture. Overall, the data suggest the release of mineralized matrix produced by differentiated stem cells, which is advantageous for titanium implant applications. Owing to increased cell proliferation, the release of mineral compounds can induce tissue regeneration at the site of implantation.

4 Conclusions

In the present study, a novel osteogenic composite nano-coating for titanium implant surfaces has been developed. This electrospun PCL/nHAp/SrRan nanocoating shows a porous structure and a composition similar to that of the natural human bone, as confirmed by chemical analyses. The novel bioactive nanocoating is not toxic to human cells and to blood. The PCL/nHAp/SrRan is suitable for the adhesion and proliferation of cells and displays osteoinductive properties. Thus, PCL/nHAp/SrRan induces the in-vitro differentiation of bone marrow derived mesenchymal stem cells into the osteogenic lineage, in terms of ALP activity and calcium release. This study also underlines the osteogenic role of SrRan in MSC behavior and its effect on calcium phosphate mineralization. Overall the findings show that electrospun PCL/nHAp/SrRan composite could be a potential candidate as a bone implant coating material. However, further animal studies will be required to evaluate key elements such as capacity for in-vivo bone healing and implant fixation.

References

[1] BOSE S, VAHABZADEH S, BANDYOPADHYAY A. Bone tissue engineering using 3D printing [J]. Materials Today, 2013, 16(12): 496−504.

[2] WU Shui-lin, LIU Xiang-mei, YEUNG K W K, LIU Chang-sheng, YANG Xian-jin. Biomimetic porous scaffolds for bone tissue engineering [J]. Materials Science and Engineering R, 2014, 80: 1−36.

[3] LIU S H, YANG R S, AL-SHAIKH R, LANE J M. Collagen in tendon, ligament, and bone healing: A current review [J]. Clinical Orthopaedics and Related Research, 1995, 318: 265−278.

[4] DIMITRIOU R, TSIRIDIS E, GIANNOUDIS P V. Current concepts of molecular aspects of bone healing [J]. Injury, 2005, 36: 1392−1404.

[5] KALFAS I H. Principles of bone healing [J]. Neurosurgical Focus, 2001, 10: 1−4.

[6] FORSTER Y, RENTSCH C, SCHNEIDERS W, BERNHARDT R, SIMON J C, WORCH H, RAMMELT S. Surface modification of implants in long bone [J]. Biomatter, 2012, 2: 149−157.

[7] WANG Guo-hui, FU Hua, ZHAO Yan-zhong, ZHOU Ke-chao, ZHU Shai-hong. Bone integration properties of antibacterial biomimetic porous titanium implants [J]. Transactions of Nonferrous Metals Society of China, 2017, 27: 2007−2014.

[8] LI Xiang, MA Xiang-yu, FENG Ya-fei, MA Zhen-sheng, WANG Jian, MA Tian-cheng, QI Wei, LEI Wei, WANG Lin. Osseointegration of chitosan coated porous titanium alloy implant by reactive oxygen species-mediated activation of the PI3K/AKT pathway under diabetic conditions [J]. Biomaterials, 2015, 36: 44−54.

[9] WANG G C, ZREIQAT H. Functional coatings or films for hard-tissue applications [J]. Materials, 2010, 3: 3994−4050.

[10] KISHAN A P, COSGRIFF-HERNANDEZ E M. Recent advancements in electrospinning design for tissue engineering applications: A review [J]. Journal of Biomedical Materials Research A, 2017, 105: 2892−2905.

[11] BUTTAFOCO L, KOLKMAN N G, ENGBERS-BUIJTENHUIJS P, POOT A A, DIJKSTRA P, VERMES I, FEIJEN J. Electrospinning of collagen and elastin for tissue engineering applications [J]. Biomaterials, 2006, 27: 724−734.

[12] INANC B, ARSLAN Y E, SEKER S, ELCIN A E, ELCIN Y M. Periodontal ligament cellular structures engineered with electrospun poly(DL-lactide-co-glycolide) nanofibrous membrane scaffolds [J]. Journal of Biomedical Materials Research A, 2009, 90: 186−195.

[13] DEMIRDOGEN B, BONILLA C E, TRUJILLO S, PERILLA J E, ELCIN A E, ELCIN Y M, RIBELLES J L G. Silica coating of the pore walls of a microporous polycaprolactone membrane to be used

in bone tissue engineering [J]. Journal of Biomedical Materials Research A, 2014, 102: 3229−3236.

[14] KHANDAKER M, RIAHINEZHAD S, JAMADAGNI H G, MORRIS T L, COLES A V, VAUGHAN M B. Use of polycaprolactone electrospun nanofibers as a coating for poly (methyl-methacrylate) bone cement [J]. Nanomaterials, 2017, 7(7): 1−16.

[15] THOMAS R, SOUMYA K R, MATHEW J, RADHAKRISHNAN E K. Electrospun polycaprolactone membrane incorporated with biosynthesized silver nanoparticles as effective wound dressing material [J]. Applied Biochemistry and Biotechnology, 2015, 176: 2213−2224.

[16] BAYKAN E, KOC A, ELCIN A E, ELCIN Y M. Evaluation of a biomimetic poly(*ε*-caprolactone)/*β*-tricalcium phosphate multispiral scaffold for bone tissue engineering: In vitro and in vivo studies [J]. Biointerphases, 2014, 9: 029011.

[17] BONILLA C E P, TRUJILLO S, DEMIRDOGEN B, PERILLA J E, ELCIN Y M, RIBELLES J L G. New porous polycaprolactone−silica composites for bone regeneration [J]. Materials Science and Engineering C, 2014, 40: 418−426.

[18] INANC B, ELCIN A E, KOC A, BALOS K, PARLAR A, ELCIN Y M. Encapsulation and osteoinduction of human periodontal ligament fibroblasts in chitosan−HA microspheres [J]. Journal of Biomedical Materials Research A, 2007, 82: 917−926.

[19] KOC A, FINKENZELLER G, ELCIN A E, STARK G B, ELCIN Y M. Evaluation of adenoviral vascular endothelial growth factor-activated chitosan/hydroxyapatite scaffold for engineering vascularized bone tissue using human osteoblasts: In vitro and in vivo studies [J]. Journal of Biomaterials Applications, 2014, 29: 748−760.

[20] HE Zheng-yuan, ZHANG Lei, SHAN Wen-rui, ZHANG Yu-qin, ZHOU Rong, JIANG Ye-hua, TAN Jun. Mechanical and corrosion properties of Ti−35Nb−7Zr−*x*HA composites fabricated by spark plasma sintering [J]. Transactions of Nonferrous Metals Society of China, 2017, 27: 848−856.

[21] ICONARU S L, PRODAN A M, BUTON N, PREDOI D. Structural characterization and antifungal studies of zinc-doped hydroxyapatite coatings [J]. Molecules, 2017, 22: 1−13.

[22] ZHAO Guo-liang, WEN Guang-wu, WU Kun. Influence of processing parameters and heat treatment on phase composition and microstructure of plasma sprayed hydroxyapatite coatings [J]. Transactions of Nonferrous Metals Society of China, 2009, 19: 463−469.

[23] PARK J W, KIM H K, KIM Y J, JANG J H, SONG H J, HANAWA T. Osteoblast response and osseointegration of a Ti−6Al−4V alloy implant incorporating strontium [J]. Acta Biomaterialia, 2010, 6: 2843−2851.

[24] ALMEIDA M M, NANI E P, TEIXEIRA L N, PERUZZO D C, JOLY J C, NAPIMOGA M H. Strontium ranelate increases osteoblast activity [J]. Tissue and Cell, 2016, 48: 183−188.

[25] IBRAHIM M R M, SINGH S, MERICAN A M, RAGHAVENDRAN H R B, MURALI M R, NAVEEN S V, KAMARUL T. The effect of strontium ranelate on the healing of a fractured ulna with bone gap in rabbit [J]. BMC Veterinary Research, 2016, 12: 1−9.

[26] MONTESI M, PANSERI S, DAPPORTO M, TAMPIERI A, SPRIO S. Sr-substituted bone cements direct mesenchymal stem cells, osteoblasts and osteoclasts fate [J]. Plos One, 2017, 12(2): e0172100.

[27] FROMIGUE O, HAY E, BARBARA A, PETREL C, TRAIFFORT E, RUAT M, MARIE P J. Calcium sensing receptor-dependent and receptor-independent activation of osteoblast replication and survival by strontium ranelate [J]. Journal of Cellular and Molecular Medicine, 2009, 13(8B): 2189−2199.

[28] YANG Fan, YANG Dan-zhi, TU Jie, ZHENG Qi-xin, CAI Lin-tao, WANG Li-ping. Strontium enhances osteogenic differentiation of mesenchymal stem cells and in vivo bone formation by activating Wnt/catenin signaling [J]. Stem Cells, 2011, 29: 981−991.

[29] PORS NIELSEN S. The biological role of strontium [J]. Bone, 2004, 35: 583−588.

[30] BONNELYE E, CHABADEL A, SALTEL F, JURDIC P. Dual effect of strontium ranelate: Stimulation of osteoblast differentiation and inhibition of osteoclast formation and resorption in vitro [J]. Bone, 2008, 42: 129−138.

[31] VEGGER J B, BRÜEL A, SØRENSEN T G, THOMSEN J S. Systemic treatment with strontium ranelate does not influence the healing of femoral mid-shaft defects in rats [J]. Calcified Tissue International, 2016, 98: 206−214.

[32] TIAN Ai, ZHAI Jun-jiang, PENG Yan, ZHANG Li, TENG Min-hua, LIAO Jian, SUN Xu, LIANG Xing. Osteoblast response to titanium surfaces coated with strontium ranelate-loaded chitosan film [J]. The International Journal of Oral & Maxillofacial Implants, 2014, 29: 1446−1453.

[33] WEI L, KE J, PRASADAM I, MIRAO R J, LIN S, XIAO Y, ZHANG Y. A comparative study of Sr-incorporated mesoporous bioactive glass scaffolds for regeneration of osteopenic bone defects [J]. Osteoporosis International, 2014, 25: 2089−2096.

[34] LI Yun-feng, LI Qing, ZHU Song-song, LUO En, LI Ji-hua, FENG Ge, LIAO Yun-mao, HU Jing. The effect of strontium-substituted hydroxyapatite coating on implant fixation in ovariectomized rats [J]. Biomaterials, 2010, 31: 9006−9014.

[35] DAHL S G, ALLAIN P, MARIE P J, MAURAS Y, BOIVIN G, CHRISTIANDEN C. Incorporation and distribution of strontium in bone [J]. Bone, 2001, 28: 446−453.

[36] WENG L, TEUSINK M J, SHULER F D, PARECKI V, XIE J W. Highly controlled coating of strontium-doped hydroxyapatite on electrospun poly(*ε*-caprolactone) fibers [J]. Journal of Biomedical Materials Research (Part B): Applied Biomaterials, 2016, 105: 753−763.

[37] LIANG Yong-qiang, LI Hao-yan, XU Jiang, LI Xin, LI Xin-chang, YAN Yu-ting, Qi Meng-chun. Strontium coating by electrochemical deposition improves implant osseointegration in osteopenic models [J]. Experimental and Therapeutic Medicine, 2015, 9: 172−176.

[38] MAÏMOUN L, BRENNAN T C, BADOUD I, DUBOIS-FERRIERE V, RIZZOLI R, AMMANN P. Strontium ranelate improves implant osseointegration [J]. Bone, 2010, 46: 1436−1441.

[39] LIU Xing, ZHU Shi-jun, CUI Jing-fu, SHAO Hong-guo, ZHANG Wen, YANG Hui-lin, XU Yao-zeng, GENG De-chun, YU Long. Strontium ranelate inhibits titanium-particle-induced osteolysis by restraining inflammatory osteoclastogenesis in vivo [J]. Acta Biomaterialia, 2014, 10: 4912−4918.

[40] SEKER S, ARSLAN Y E, ELÇIN Y M. Electrospun nanofibrous PLGA/fullerene-C60 coated quartz crystal microbalance for real-time gluconic acid monitoring [J]. IEEE Sensors Journal, 2010, 10: 1342−1348.

[41] CELEBI B, ELCIN Y M. Proteome analysis of rat bone marrow mesenchymal stem cell subcultures [J]. Journal of Proteome Research, 2009, 8: 2164−2172.

[42] CELEBI B, ELCIN A E, ELCIN Y M. Proteome analysis of rat bone marrow mesenchymal stem cell differentiation [J]. Journal of Proteome Research, 2010, 9: 5217−5227.

[43] VENUGOPAL J, LOW S, CHOON A T, KUMAR A B, RAMAKRISHNA S. Electrospun-modified nanofibrous scaffolds for the mineralization of osteoblast cells [J]. Journal of Biomedical Materials Research, 2007, 84: 408−417.

[44] CAMARGO N H A, de LIMA S A, GEMELLI E. Synthesis and characterization of hydroxyapatite/TiO_2 nanocomposites for bone tissue regeneration [J]. American Journal of Biomedical Engineering, 2012, 2: 41−47.

[45] GARKHAL K, VERMA S, JONNALAGADDA S, KUMAR N. Fast degradable poly(*L*-lactide-co-ecaprolactone) microspheres for tissue engineering: Synthesis, characterization, and degradation behavior [J]. Journal of Polymer Science (Part A), 2007, 45: 2755−2764.

[46] QIAN Yong-fang, ZHANG Zhen, ZHENG Lai-jiu, SONG Ruo-yuan, ZHAO Yu-ping. Fabrication and characterization of electrospun polycaprolactone blended with chitosan−gelatin complex nanofibrous mats [J]. Journal of Nanomaterials, 2014, 2014: 964621.

[47] ZEITZ C, FAIDT T, GRANDTHYLL S, HAHL H, THEWES N, SPENGLER C, HANNIG M. Synthesis of hydroxyapatite substrates: Bridging the gap between model surfaces and enamel [J]. ACS Applied Materials & Interfaces, 2016, 8: 25848−25855.

[48] HOIDY W H, AHMAD M B, AL-MULLA E A J, IBRAHIM N A B. Preparation and characterization of polylactic acid/polycaprolactone clay nanocomposites [J]. Journal of Applied Sciences, 2010, 10: 97−106.

[49] ELZEIN T, NASSER-EDDINE M, DELAITE C, BISTAC S, DUMAS P. FTIR study of polycaprolactone chain organization at interfaces [J]. Journal of Colloid and Interface Science, 2004, 273: 381−387.

[50] CHEN M, LE D Q S, KJEMS J, BUNGER C, LYSDAHL H. Improvement of distribution and osteogenic differentiation of human mesenchymal stem cells by hyaluronic acid and *β*-tricalcium phosphate-coated polymeric scaffold in vitro [J]. BioResearch Open Access, 2015, 4: 363−373.

[51] QUERIDO W, FARINA M. Strontium ranelate increases the formation of bone-like mineralized nodules in osteoblast cell cultures and leads to Sr incorporation into the intact nodules [J]. Cell and Tissue Research, 2013, 354: 573−580.

[52] GOMEZ B, ARDAKANI S, JU J, JENKINS D, CERELLI M J, DANILOFF G Y, KUNG V T. Monoclonal antibody assay for measuring bone-specific alkaline phosphatase activity in serum [J]. Clinical Chemistry, 1995, 41: 1560−1566.

基于纳米羟基磷灰石、雷尼酸锶和聚己内酯的钛植入体成骨纳米复合涂层

Murat Taner VURAT[1,2], Ayşe Eser ELÇIN[1], Yaşar Murat ELÇIN[1,2]

1. Tissue Engineering, Biomaterials and Nanobiotechnology Laboratory, Faculty of Science and Stem Cell Institute, Ankara University, Ankara 06100, Turkey;
2. Biovalda Health Technologies, Inc., Ankara 06830, Turkey

摘　要：钛及其合金常被用作牙科和骨植入材料。钛表面的仿生涂层可以改善其成骨性能。本文作者开发一种新型的、具有成骨作用的钛合金表面纳米复合涂层，为骨髓间充质干细胞(MSCs)的粘附、增殖和成骨分化提供自然环境。用静电纺丝法制备基于聚己内脂(PCL)、纳米羟基磷灰石 (nHAp)和雷尼酸锶 (SrRan)的纳米复合涂层。因此，涂覆在钛合金表面的涂层有 4 种，分别为 PCL、PCL/nHAp、PCL/SrRan 和 PCL/nHAp/SrRan。采用 EDS、FTIR、XRD、XRF、SEM、AFM、体外细胞毒性和血液相容性测试等技术评估涂层的化学性能、形貌和生物学性能。结果表明，纳米复合涂层具有细胞相容性和血液相容性，PCL/HAp/SrRan 纳米复合纤维涂层具有最高的细胞活性。MSCs 在纳米涂层上的成骨培养显示干细胞向成骨分化，碱性磷酸酶活性和矿化测试结果证实了这一点。研究结果表明，所制备的复合纳米涂层具有促进新骨形成和增强骨−植入体整合的潜力。

关键词：成骨纳米涂层；复合纳米纤维；钛植入体；纳米羟基磷灰石；雷尼酸锶；聚己内酯；静电纺丝；间充质干细胞

(Edited by Wei-ping CHEN)